

1
2
3
4
5
6
7
8
9
10
11
12
13
14
15
16
17
18

Novel Immunoglobulin Domain Proteins Provide Insights into Evolution and Pathogenesis Mechanisms of SARS-Related Coronaviruses

Yongjun Tan^a, Theresa Schneider^a, Matthew Leong^b, L Aravind^c, Dapeng Zhang^{a,d,*}

^a Department of Biology, College of Arts and Sciences, Saint Louis University, MO 63110

^b School of Medicine, Saint Louis University, MO 63110

^c National Center for Biotechnology Information, National Library of Medicine, National Institutes of Health, Bethesda, MD 20894

^d Program of Bioinformatics and Computational Biology, College of Arts and Sciences, Saint Louis University, MO 63110

*Corresponding Author: Dapeng Zhang, Ph.D. (dapeng.zhang@slu.edu)

19 **ABSTRACT**

20 A novel coronavirus (SARS-CoV-2) is the causative agent of an emergent severe respiratory disease
21 (COVID-19) in humans that is threatening to result in a global health crisis. By using genomic, sequence,
22 structural and evolutionary analysis, we show that Alpha- and Beta-CoVs possess several novel families
23 of immunoglobulin (Ig) domain proteins, including ORF8 and ORF7a from SARS-related coronaviruses
24 and two protein groups from certain Alpha-CoVs. Among them, ORF8 is distinguished in being rapidly
25 evolving, possessing a unique insert and a hypervariable position among SARS-CoV-2 genomes in its
26 predicted ligand-binding groove. We also uncover many Ig proteins from several metazoan viruses
27 which are distinct in sequence and structure but share an architecture comparable to that of CoV Ig
28 domain proteins. Hence, we propose that deployment of Ig domain proteins is a widely-used strategy by
29 viruses, and SARS-CoV-2 ORF8 is a potential pathogenicity factor which evolves rapidly to counter the
30 immune response and facilitate the transmission between hosts.

31

32 **KEYWORDS** Coronavirus, COVID-19, SARS, ORF8, Immunoglobulin, Evolution, Pathogenicity, Immune
33 evasion

34 **Introduction**

35 Nidoviruses are an ancient group of lipid-enveloped viruses with non-segmented RNA genomes, which
36 are known to infect oomycetes and animals, including molluscs, arthropods and vertebrates (1). Among
37 them are the coronaviruses (CoVs) which possess the largest known monopartite RNA genomes and are
38 classified into four genera—Alphacoronavirus, Betacoronavirus, Gammacoronavirus, and
39 Deltacoronavirus (2). Over the past two decades, Beta-CoVs, including the viruses responsible for
40 Severe Acute Respiratory Syndrome (SARS) in 2003 and Middle Eastern Respiratory Syndrome (MERS) in
41 2012, have emerged as significant local and global health concerns with economic consequences (3, 4).
42 Recently, a novel severe respiratory disease has emerged in humans (abbreviated COVID-19) (5, 6).
43 COVID-19 presents with a relatively long incubation period of 1-2 weeks followed by development of
44 fever, dry cough, dyspnea and bilateral ground-glass opacities in the lungs (7). In some patients, this can
45 proceed to fatal respiratory failure, characterized by acute lung injury (8) and acute respiratory distress
46 syndrome (9). Within several months of the first outbreak, there have been over 75,000 confirmed cases
47 with over 2,000 deaths of COVID-19 globally ([https://www.who.int/docs/default-](https://www.who.int/docs/default-source/coronaviruse/situation-reports/20200220-sitrep-31-covid-19.pdf)
48 [source/coronaviruse/situation-reports/20200220-sitrep-31-covid-19.pdf](https://www.who.int/docs/default-source/coronaviruse/situation-reports/20200220-sitrep-31-covid-19.pdf)). Due to the rapid spread and
49 potential severity of the disease, COVID-19 poses as a potential major threat to human health. A novel
50 coronavirus (SARS-CoV-2) was identified as the causative agent of COVID-19, and phylogenomic analysis
51 has shown that it belongs to the same larger clade of Beta-CoVs as the SARS-CoV with a likely origin in
52 bats (5, 10, 11). Despite intense scrutiny, multiple proteins encoded by the SARS-related CoV (including
53 SARS-CoV-2) genome remain enigmatic. Here, we present a computational and evolutionary analysis to
54 show that one such mysterious protein, ORF8, and several others from Alpha- and Beta-coronavirus,
55 comprise novel families of immunoglobulin domain proteins, which might function as potential
56 modulators of host immunity to delay or attenuate the immune response against the viruses.

57

58 **Materials and methods**

59 ***Genome comparison analysis***

60 We retrieved the SARS-related CoV genomes by searching against the non-redundant (nr) nucleotide
61 database of the National Center for Biotechnology Information (NCBI) with the SARS-CoV-2 genome
62 sequence (NC_045512.2) as a query (12). The program CD-HIT was used for similarity-based clustering
63 (13). A multiple sequence alignment of whole virus genomes was performed by KALIGN (14). Based on
64 the MSA, a similarity plot was constructed by a custom Python script, which calculated the identity
65 between each subject sequence and the SARS-CoV-2 genome sequence based on a custom sliding

66 window size and step size. Open reading frames of virus genomes used in this study were extracted
67 from an NCBI Genbank file.

68

69 ***Protein sequence analysis***

70 To collect protein homologs, iterative sequence profile searches were conducted by the programs PSI-
71 BLAST (Position-Specific Iterated BLAST)(12) and JACKHMMER (15), which searched against the non-
72 redundant (nr) protein database of NCBI with a cut-off e-value of 0.005 serving as the significance
73 threshold. Similarity-based clustering was conducted by BLASTCLUST, a BLAST score-based single-linkage
74 clustering method (<ftp://ftp.ncbi.nih.gov/blast/documents/blastclust.html>). Multiple sequence
75 alignments were built by the KALIGN (14), MUSCLE(16) and PROMALS3D(17) programs, followed by
76 careful manual adjustments based on the profile–profile alignment, the secondary structure information
77 and the structural alignment. Profile-profile comparison was conducted using the HHpred program (18).
78 The consensus of the alignment was calculated using a custom Perl script. The alignments were colored
79 using an in-house alignment visualization program written in perl and further modified using adobe
80 illustrator. Signal peptides were predicted by the SignalP-5.0 Server (19). The transmembrane regions
81 were predicted by the TMHMM Server v. 2.0 (20).

82

83 ***Identification of distinct viral Ig domain proteins***

84 By using the protein remote relationship detection methods, we generated a collection of distinct Ig
85 domains from the Pfam database (21) and also from our local domain database. Then, we utilized the
86 hmmscan program of the HMMER package (22) and RPS-BLAST (12, 23) to retrieve the homologs from
87 viral genomes.

88

89 ***Molecular Phylogenetic analysis***

90 The evolutionary history was inferred by using the Maximum Likelihood method based on the JTT
91 w/freq. model (24). The tree with the highest log likelihood is shown. Support values out of 100
92 bootstraps are shown next to the branches (25). Initial tree(s) for the heuristic search were obtained
93 automatically by applying Neighbor-Join and BioNJ algorithms to a matrix of pairwise distances
94 estimated using a JTT model, and then selecting the topology with the superior log likelihood value. A
95 discrete Gamma distribution was used to model evolutionary rate differences among sites (4
96 categories). The rate variation model allowed for some sites to be evolutionarily invariable. The tree is

97 drawn to scale, with branch lengths measured in the number of substitutions per site. The tree diagram
98 was generated using MEGA Tree Explorer (26)

99

100 ***Entropy analysis***

101 Position-wise Shannon entropy (H) for a given multiple sequence alignment was calculated using the
102 equation:

$$H = - \sum_{i=1}^M P_i \log_2 P_i$$

103

104 P is the fraction of residues of amino acid type i , and M is the number of amino acid types. The Shannon
105 entropy for the i th position in the alignment ranges from 0 (only one residue at that position) to 4.32 (all
106 20 residues equally represented at that position). Analysis of the entropy values which were thus
107 derived was performed using the R language.

108

109 ***Protein Structure Prediction and Analysis***

110 The secondary structural prediction was conducted using the Jnet (Joint Network) program (27). Jnet is a
111 neural network-based predictor which trains neural networks from three different types of profiles:
112 profile PSSM, profile HMM, and residue frequency profile. It generates a consensus secondary structure
113 with an average accuracy of 72% or greater.

114

115 The Modeller9v1 program (Sali and Blundell, 1993) was utilized for homology modeling of structure of
116 SARS-CoV-2 ORF8 using the SARS-CoV ORF7 (1xak_A) (28) as a template. Since in these low sequence-
117 identity cases, sequence alignment is the most important factor affecting the quality of the model
118 (Cozzetto and Tramontano, 2005), alignments used in this study have been carefully built and cross-
119 validated based on the information from HHpred and edited manually using the secondary structure
120 information. We generated five models and selected the one that had better model accuracy p-value
121 and global model quality score as assessed by ModFOLD6 online server (29). Structural analysis and
122 comparison were conducted using the molecular visualization program PyMOL (30). The structural
123 similarity search was performed using the DALI server (31).

124

125 **Results and discussion**

126 ***Comparative genomics unveils fast-evolving regions of SARS-related CoV genomes***

127 The host-pathogen arms-race has selected for a disparate complement of viral genes involved in
128 pathogenesis. These genes often rapidly diversify through recombination and mutations to keep up with
129 the evolution of host resistance. To identify proteins with potential pathogenic roles in COVID-19, we
130 conducted a comparative genomic analysis of the coronaviruses. Similarity plots show that the bat CoV
131 RaTG13 is the closest relative of SARS-CoV-2 with no evidence for recombination between them (Figure
132 1 and Figure S1). SARS-CoV-2 also shows good similarity to two other bat viruses, CoVZXC21 and
133 CoVZXC45, first in the 5' half of ORF1 and again after nucleotide number 20,000 of the genome.
134 However, the remaining part of ORF1 of SARS-CoV-2 and RaTG13 show no specific relationship to these
135 viruses. This suggests a recombination event between the common ancestor of SARS-CoV-2 and RaTG13,
136 and probably another member of the SARS-related clade close to CoVZXC21 and CoVZXC45. In addition
137 to this major recombination event, we identified several smaller regions which might have undergone
138 recombinational diversification during the emergence of the SARS-CoV-2 genome (Figure S1). Notably,
139 many of them are clustered in three regions displaying extensive diversification, corresponding to the N-
140 terminal region of the ORF1a polyprotein, the Spike protein, and the uncharacterized protein encoded
141 by ORF8 (Figure 1 and Figure S1).

142

143 ***Identification of novel immunoglobulin protein families in CoVs***

144 Among these three fast-evolving proteins, we focused on the ORF8 protein as it is one of the so-called
145 accessory proteins, which does not participate in viral replication (32, 33), raising the possibility that it
146 might have a role in viral pathogenesis. It is a predicted secreted protein present only in some Beta-
147 CoVs, including SARS-CoV-2 but not the MERS-like clade. Profile-profile comparisons using a sequence-
148 profile built from the multiple sequence alignment of all available ORF8 proteins showed it to be
149 unexpectedly homologous to the membrane-anchored ORF7a protein from the same subset of Beta-
150 CoVs, and several proteins (variously annotated as ORF9 or ORF10) from a subset of bat Alpha-CoVs
151 (Figure 2A) (probability=94% of profile-profile match) (34). ORF7a is a known member of the
152 immunoglobulin (Ig) domain superfamily and is specifically related to extracellular metazoan Ig domains
153 that are involved in adhesion, such as ICAM (35, 36). The Beta-CoV ORF8, ORF7a and the Alpha-CoV Ig
154 domains display a classic β -sandwich fold with seven β -stands and share the characteristic pattern of
155 two cysteines which form stabilizing disulfide bonds with metazoan Ig domains (Figure 2A and Figure S2)
156 (37). However, they are unified as a clade by the presence of an additional pair of conserved disulfide-
157 bonding cysteines (Figure 2A). Nonetheless, there are notable structural differences between the three
158 groups of proteins. ORF8 is distinguished from ORF7a and Alpha-CoV Ig proteins by the loss of the C-

159 terminal transmembrane (TM) helix and the acquisition of a long insert between stands 3 and 4 with a
160 conserved cysteine which might facilitate dimerization through disulfide-bond formation (Figure 2A).
161 The homology model of ORF8, based on the structure of SARS-CoV ORF7a (pdb id:1XAK), suggests that
162 this insert augments a potential peptide-ligand binding groove that has been proposed for ORF7a
163 (Figure 2B and Figure S3). Hence, the emergence of the insert has gone hand-in-hand with the
164 acquisition of a modified interaction interface.

165
166 Besides these families, we identified a fourth family of Ig domains from the same Alpha-CoVs which
167 contain the above-discussed ORF7a/8-like Ig family (Figure 3A). These Alpha-CoVs typically possess one
168 or two paralogous copies annotated as either ORF4a/b or NS5a/b. From their sequences, these Ig
169 domains are not closely related to the ORF7a and ORF8 Ig domains (Figure S4). However, profile-profile
170 searches have shown that they are related to Ig domains found in the adenoviral E3-CR1 proteins
171 (probability: 90% of matching the Pfam CR1 Ig domain profile) (Figure S4). In these searches, they also
172 yield weaker hits to two other Ig domains, namely the poxviral decoy interferon receptors and human T-
173 cell surface CD3 zeta (Figure S4).

174

175 ***ORF8 is a fast-evolving protein in SARS-related CoVs***

176 Phylogenetic analysis of ORF7a, ORF8 and Alpha-CoV Ig domains shows that each group represents a
177 distinct clade (Figure 2C). The tree topology of ORF7a mirrors that of the polymerase tree (Figure 3A);
178 however, the topology of the ORF8-Ig clade is not consistent with it. This might be due to a
179 recombination event between the SARS-related CoVs (as suggested by the similarity plot analysis)
180 and/or unusual divergence under selection. To better understand the functional difference between
181 ORF8 and ORF7a, we examined the column-wise Shannon entropy in the 20 amino acid alphabet and
182 found that the ORF8 has significantly higher mean entropy than ORF7a (ORF8: 1.09 vs ORF7a: 0.22, $p <$
183 10^{-16} for the H_0 of congruent means by t-test) (Figure 2D). By comparing column-wise entropies in both
184 the 20 amino acid and a reduced 8-letter alphabet (where amino acids are grouped based on similar
185 side-chain chemistry), we found at least 14 positions in ORF8 which show high entropy in both alphabets
186 as compared to a single position in ORF7a (Figure 2D). This indicates that ORF8 is a fast-evolving protein
187 under selection for diversity as contrast to ORF7a. Strikingly, one of these highly variable positions,
188 which features residues with very different side characters (hydrophobic, acidic, alcoholic and proline),
189 corresponding to Leu84 was also identified as the most variable position across 54 closely related
190 human SARS-CoV-2 genome sequences (38). In our structural model, this residue is positioned at the

191 predicted peptide-ligand binding groove of the ORF8-Ig domain (Figure 2B). Therefore, our entropy and
192 structural analysis of the ORF8-Ig domain, in conjunction with its hypervariable position found in human
193 SARS-CoV-2 genomes, points to a role for ORF8 at the interface of the host-virus interaction possibly in a
194 pathogenic context.

195

196 ***Ig domain proteins are newly acquired in subsets of Alpha- and Beta-CoVs***

197 We examined the distribution of CoV Ig proteins in the context of a phylogenetic tree of both Beta-and
198 Alpha-CoVs based on their polymerase proteins (Figure 3A). Other than the two subsets of Beta-CoVs
199 and Alpha-CoVs that contain the above-described Ig domain proteins, no other CoVs contain any Ig
200 domain proteins (Figure 3A). The immediate sister-groups of the Ig-containing CoVs typically have Spike,
201 E, M and N, and one or two other uncharacterized accessory proteins which are not Ig domains to our
202 best knowledge. The Alpha-CoV ORF9/10 share a C-terminal TM helix and, along with ORF7a of the Beta-
203 CoVs, lack the insert in the Ig domain (Figure 2A). Hence, it is possible that this architecture represents
204 the ancestral state which was present in the common ancestor of both Alpha-CoVs and Beta-CoVs.

205 Under this scenario, the protein was displaced/lost both in certain Alpha-CoVs and Beta-CoVs.

206 Alternatively, ORF7a could have been exchanged between Alpha- and Beta-CoVs by a recombination
207 event. In both scenarios, ORF8 arose likely via a duplication of ORF7a in specifically the Beta-CoVs.

208 Although we couldn't identify the ultimate precursors of the CoV Ig domains, they are likely to have
209 been acquired on at least two independent occasions from different sources. The CoV ORF7a-ORF8
210 families might have derived from the metazoan adhesion Ig families, and the ORF4a/b-like Ig domains of
211 Alpha-CoVs were likely acquired from adenoviral CR1 Ig domains with which they share some specific
212 sequence features.

213

214 ***Divergent Ig proteins with a comparable architecture are deployed by distinct viruses***

215 The presence of multiple Ig domains with different affinities in CoVs prompted us to more generally
216 survey animal viruses for Ig domains. By using the Pfam models (39) and our own PSSMs created from
217 PSI-BLAST runs with Ig domains (12), we were able to identify about 17 distinct viral Ig domain families
218 in a wider diversity of animal viruses (Figure 3B and Table S2). In addition to CoVs, such Ig domain
219 proteins can be found in adenoviruses, NCLDVs, Herpesviruses and Phenuiviruses. These viral Ig domains
220 are highly divergent; many of them are only found in certain viral groups. However, the majority have an
221 architecture comparable to the CoV-Ig domains, with an N-terminal signal peptide, one or multiple Ig
222 domains and a C-terminal TM region often followed by a stretch of basic residues. Thus, although the Ig

223 domains are not the universally preserved component of viruses, they have been acquired and selected
224 independently by a wide range of viruses. The presence of a proofreading 3'-5' exonuclease has been
225 proposed to favor the emergence of larger RNA genomes in CoVs (40). Indeed, this might have also
226 contributed to the acquisition of potential pathogenesis factors such as the Ig domains described herein
227 which are comparable to those seen in DNA viruses.

228

229 ***Novel CoV Ig domain proteins are potential immune modulators***

230 Why have diverse viruses independently acquired the Ig domain during their evolution? First, the Ig
231 domains are major mediators of adhesive interactions in both eukaryotes and prokaryotes (37, 41, 42).
232 Thus, this domain can be used for adherence for cell to cell spread (e.g. herpesviral Ig domain proteins)
233 (43). Further, Ig domains are major building blocks of metazoan immune systems. Thus, viruses often
234 utilize this domain to disrupt immune signaling of the host. For example, in adenoviruses, the CR1 Ig
235 domain proteins have been shown to block the surface expression on infected cells of class I major
236 histocompatibility complex molecules by blocking their trafficking from the endoplasmic reticulum (ER)
237 to Golgi (44). This has been shown to affect the host inflammatory response and modulates the
238 presentation of viral antigens to T-cells (45). In poxvirus, the secreted Ig domain proteins function as
239 interferon receptors or decoys that bind the interferon- α/β and disrupt signaling via the endogenous
240 host receptors (46). Further, SARS-ORF7a has been implicated in the interaction with bone marrow
241 stromal antigen 2 (BST-2), which tethers budding virions to the host cell in a broad-spectrum antiviral
242 response, to prevent the N-linked glycosylation of BST-2 thereby crippling the host response against the
243 virus (47). Given their shared evolutionary history and similar sequence and structural features, we
244 predict that the newly identified CoV Ig domain proteins, such as ORF8 of SARS-CoV-2, might similarly
245 function as immune modulators.

246

247 While ORF8 is a paralog of ORF7a, its lack of the TM segment, unique insert and significantly more rapid
248 evolution suggest that it has acquired a distinct function and has been under strong positive selection
249 One possible mechanism is that, like the adenoviral CR1 proteins, it interferes with MHC molecules to
250 attenuate antigen presentation, resulting in ineffective detection of the virus by the host immune
251 system. Consistent with this, the SARS-CoV ortholog translocates to the ER (48) and its higher variability
252 indicates probable selection due to its interaction with a rapidly evolving host molecule. Notably, while
253 the SARS-CoV ORF8 isolates from civets and early stages of the human epidemic are intact, it split up
254 into two ORFs (ORF8a and ORF8b) during the subsequent human epidemic (49). ORF8a and ORF8b

255 retain the conserved Cys residues of the Ig domain and have been observed to form a complex in a
256 yeast-two hybrid interaction study (50). This suggests it might still fold into an intact structure held by
257 the two disulfide bonds formed by four conserved Cys residues.

258

259 In conclusion, the presence of fast-evolving ORF8 Ig domain proteins in the SARS-related viruses,
260 including the emergent 2019 SARS-CoV-2, suggests that they might be potential pathogenicity factors
261 which counter or attenuate the host immune response and might have facilitated the transmission
262 between hosts. We hope that the discovery and analyses of the novel Ig domain proteins reported here
263 will help the community better understand the evolution and pathogenesis mechanisms of these
264 coronaviruses.

265

266

267 **Acknowledgments**

268 Y.T., T. S., M.L., and D. Z. were supported by Saint Louis University start-up fund. L.A. was supported by
269 the Intramural Research Program of the NIH, National Library of Medicine.

270

271 **Disclosure statement**

272 The authors declare no competing interests.

273

274

275 Figures

276 Figure 1. Genome comparison analysis of SARS-related CoVs.

277 Similarity plot of SARS-related CoVs against human SARS-CoV-2 Wuhan-Hu-1 genome (NC_045512.2),
278 based on a multiple sequence alignment of the whole genomes. Each point represents the percent
279 identity of a 200 bp window of the alignment with a 50 bp step size between each point. The open
280 reading frames of the SARS-CoV-2 genome (NC_045512.2) are shown above the plot. Each colored line
281 corresponds to the nucleotide similarity between the human SARS-CoV-2 genome (NC_045512.2) and
282 the respective SARS-related CoV genome. The red arrows and dashed line surround a region displaying
283 major divergence due to possible recombination within SARS-related CoV genomes. The regions marked
284 by a solid red line highlight fast-evolving regions among the SARS-related CoV genomes. For detailed
285 information about the genomes that were used in this study, refer to Table S1.

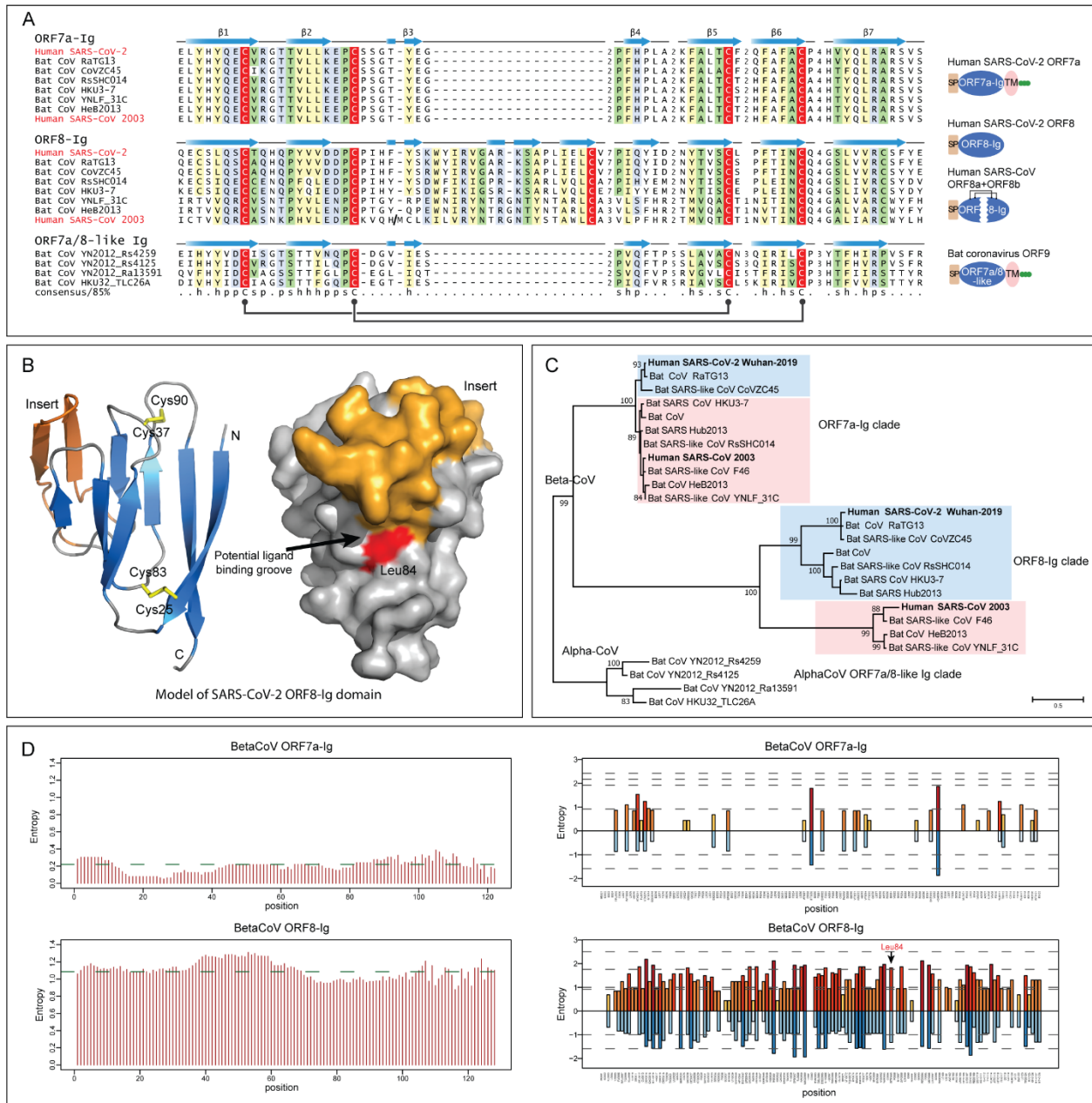


286

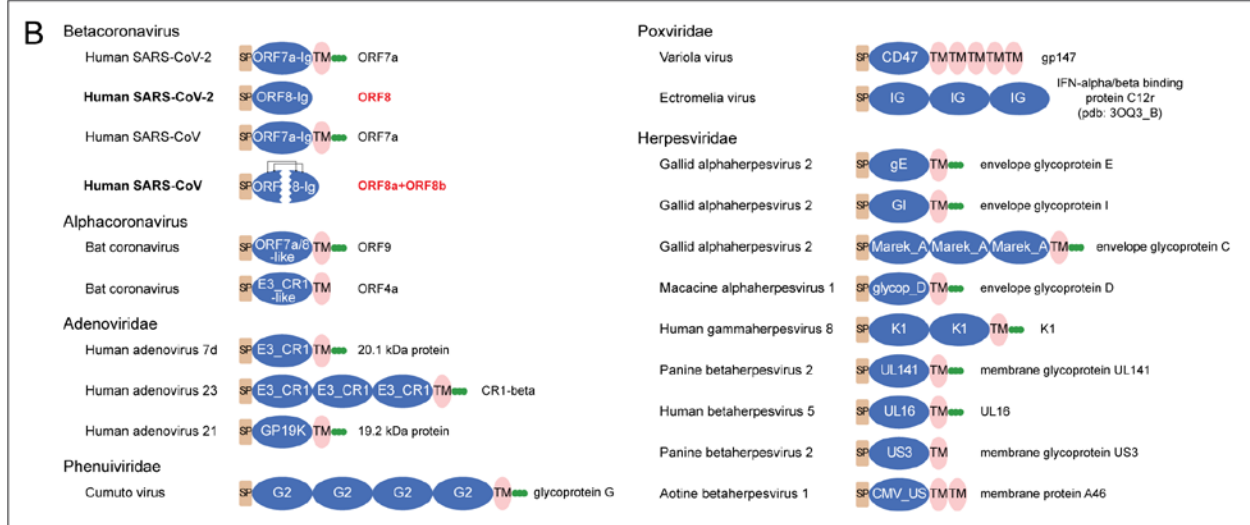
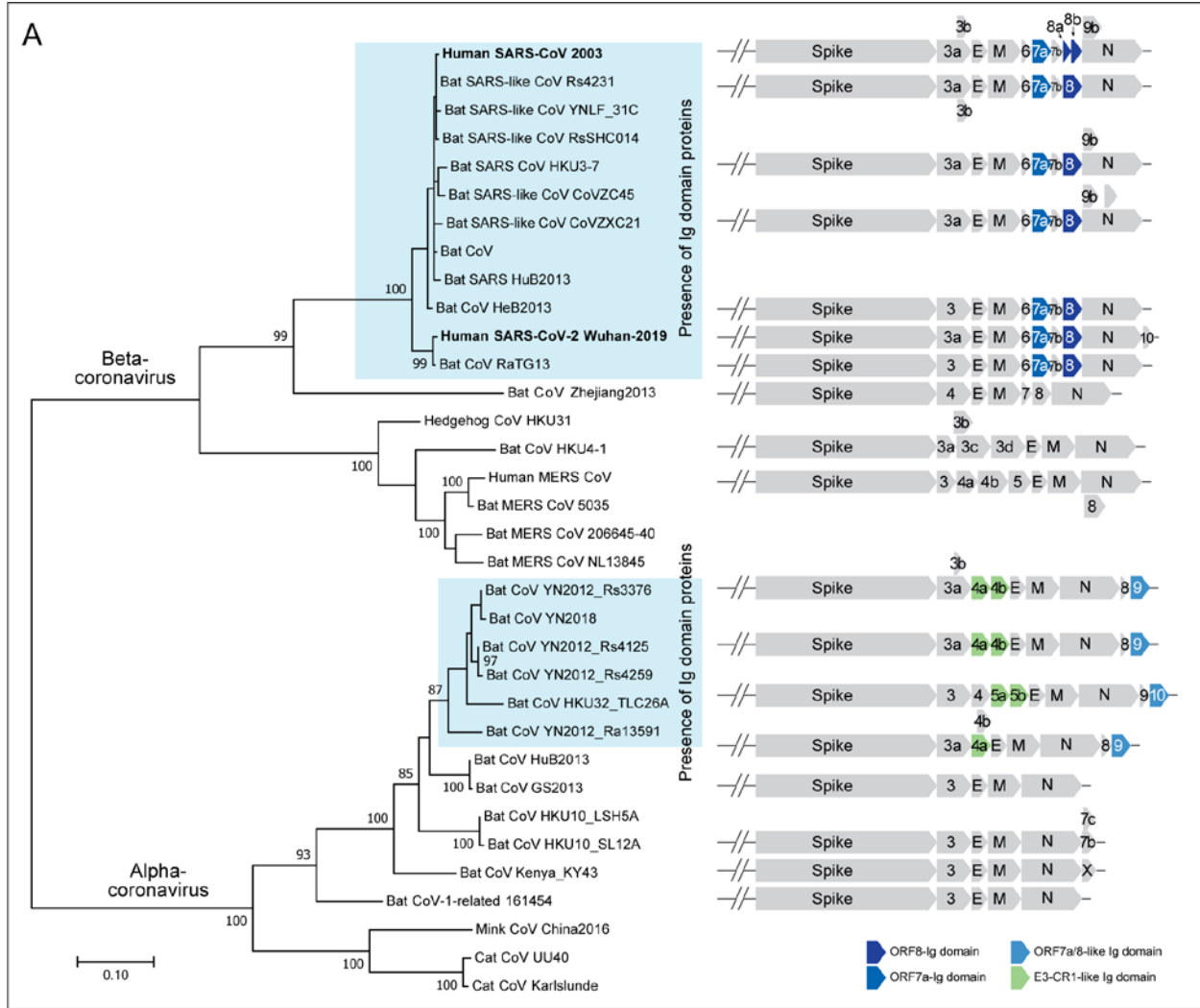
287 **Figure 2. Sequence, structure and evolutionary analysis of novel Ig domain proteins in SARS-related**
288 **CoVs.**

289 (A) Multiple sequence alignment (MSA) and representative domain architectures of ORF7a-Ig, ORF8-Ig,
290 and ORF7a/8-like Ig domain families. Each sequence in the MSA was labelled by its species abbreviation
291 followed by its source. The predicted secondary structure is shown above each alignment and the
292 consensus is shown below the super-alignment, where h stands for hydrophobic residues, s for small
293 residues, and p for polar residues. Two pairs of conserved cysteines that form disulfide bonds are
294 highlighted in red. (B) Homology model of SARS-CoV-2 ORF8-Ig domain (YP_009724396.1) and the
295 location of the hypervariable position corresponding to Leu84 in the predicted ligand-binding groove.
296 The β -sheets of the common core of the Ig fold are colored in blue, the insert in ORF8-Ig in orange and
297 the loops in grey. The characteristic disulfide bonds are highlighted in yellow. (C) Maximum likelihood
298 phylogenetic analysis of CoV Ig domain families. Support values out of 100 bootstraps are shown for the
299 major branches only. (D) Entropy plot for the ORF7a and ORF8 proteins in betacoronavirus. Left:
300 Shannon entropy computed for each column for a character space of 20 amino acids and presented as
301 mean entropy in a sliding window of 30 residues. The mean entropy across the entire length of the
302 protein is indicated as a green horizontal line. Right: Shannon entropy in regular amino acid alphabet (20
303 amino acids) are shown above the zero line in shades of orange. Shannon entropy in a reduced alphabet
304 of 8 residues are shown below the zero line in shades of blue. If a position shows high entropy in both
305 alphabets it is a sign of potential positive selection at those positions for amino acids of different
306 chemical character.

307



309 **Figure 3.** (A) Genomic structure analysis of SARS-related CoVs. The tree of coronavirus was built based
310 on an MSA of a coronavirus RNA-directed, RNA polymerase domain using a maximum likelihood model.
311 Supporting values from 100 bootstraps are shown for the major branches only. The genome structure of
312 major representative CoVs are shown right to the terminal clade of the phylogenetic tree. (B)
313 Representative domain architectures of the Ig components in different animal viruses. Proteins were
314 grouped based on their families, except for proteins of coronavirus, which were grouped based on their
315 genus. For the information of the NCBI accession numbers, refer to the supplementary data.



317 **References**

- 318 1. S. Perlman, T. Gallagher, E. J. Snijder, *Nidoviruses*. (ASM Press, Washington, DC, 2008), pp. xvi,
319 433 p.
- 320 2. J. Cui, F. Li, Z. L. Shi, Origin and evolution of pathogenic coronaviruses. *Nat Rev Microbiol* **17**,
321 181-192 (2019).
- 322 3. M. A. Marra *et al.*, The Genome sequence of the SARS-associated coronavirus. *Science* **300**,
323 1399-1404 (2003).
- 324 4. A. M. Zaki, S. van Boheemen, T. M. Bestebroer, A. D. Osterhaus, R. A. Fouchier, Isolation of a
325 novel coronavirus from a man with pneumonia in Saudi Arabia. *N Engl J Med* **367**, 1814-1820
326 (2012).
- 327 5. P. Zhou *et al.*, A pneumonia outbreak associated with a new coronavirus of probable bat origin.
328 *Nature*, (2020).
- 329 6. N. Zhu *et al.*, A Novel Coronavirus from Patients with Pneumonia in China, 2019. *N Engl J Med*,
330 (2020).
- 331 7. N. Chen *et al.*, Epidemiological and clinical characteristics of 99 cases of 2019 novel coronavirus
332 pneumonia in Wuhan, China: a descriptive study. *Lancet* **395**, 507-513 (2020).
- 333 8. J. P. Kanne, Chest CT Findings in 2019 Novel Coronavirus (2019-nCoV) Infections from Wuhan,
334 China: Key Points for the Radiologist. *Radiology*, 200241 (2020).
- 335 9. C. Huang *et al.*, Clinical features of patients infected with 2019 novel coronavirus in Wuhan,
336 China. *Lancet* **395**, 497-506 (2020).
- 337 10. D. Paraskevis *et al.*, Full-genome evolutionary analysis of the novel corona virus (2019-nCoV)
338 rejects the hypothesis of emergence as a result of a recent recombination event. *Infect Genet*
339 *Evol* **79**, 104212 (2020).
- 340 11. L. Zhang, F. M. Shen, F. Chen, Z. Lin, Origin and evolution of the 2019 novel coronavirus. *Clin*
341 *Infect Dis*, (2020).
- 342 12. S. F. Altschul *et al.*, Gapped BLAST and PSI-BLAST: a new generation of protein database search
343 programs. *Nucleic acids research* **25**, 3389-3402 (1997).
- 344 13. W. Li, A. Godzik, Cd-hit: a fast program for clustering and comparing large sets of protein or
345 nucleotide sequences. *Bioinformatics* **22**, 1658-1659 (2006).
- 346 14. T. Lassmann, E. L. Sonnhammer, Kalign—an accurate and fast multiple sequence alignment
347 algorithm. *BMC bioinformatics* **6**, 298 (2005).
- 348 15. S. R. Eddy, in *Genome Informatics 2009: Genome Informatics Series Vol. 23*. (World Scientific,
349 2009), pp. 205-211.
- 350 16. R. C. Edgar, MUSCLE: multiple sequence alignment with high accuracy and high throughput.
351 *Nucleic acids research* **32**, 1792-1797 (2004).
- 352 17. J. Pei, B.-H. Kim, N. V. Grishin, PROMALS3D: a tool for multiple protein sequence and structure
353 alignments. *Nucleic acids research* **36**, 2295-2300 (2008).
- 354 18. J. Söding, A. Biegert, A. N. Lupas, The HHpred interactive server for protein homology detection
355 and structure prediction. *Nucleic acids research* **33**, W244-W248 (2005).
- 356 19. L. Holm, S. Kääriäinen, P. Rosenström, A. Schenkel, Searching protein structure databases with
357 DaliLite v. 3. *Bioinformatics* **24**, 2780-2781 (2008).
- 358 20. J. J. A. Armenteros *et al.*, SignalP 5.0 improves signal peptide predictions using deep neural
359 networks. *Nature biotechnology* **37**, 420-423 (2019).
- 360 21. A. Krogh, B. Larsson, G. Von Heijne, E. L. Sonnhammer, Predicting transmembrane protein
361 topology with a hidden Markov model: application to complete genomes. *Journal of molecular*
362 *biology* **305**, 567-580 (2001).

- 363 22. S. El-Gebali *et al.*, The Pfam protein families database in 2019. *Nucleic acids research* **47**, D427-
364 D432 (2019).
- 365 23. A. Krogh, M. Brown, I. S. Mian, K. Sjolander, D. Haussler, Hidden Markov models in
366 computational biology. Applications to protein modeling. *Journal of molecular biology* **235**,
367 1501-1531 (1994).
- 368 24. A. Marchler-Bauer *et al.*, CDD: a database of conserved domain alignments with links to domain
369 three-dimensional structure. *Nucleic acids research* **30**, 281-283 (2002).
- 370 25. D. T. Jones, W. R. Taylor, J. M. Thornton, The rapid generation of mutation data matrices from
371 protein sequences. *Bioinformatics* **8**, 275-282 (1992).
- 372 26. J. Felsenstein, Confidence limits on phylogenies: an approach using the bootstrap. *Evolution* **39**,
373 783-791 (1985).
- 374 27. S. Kumar, G. Stecher, K. Tamura, MEGA7: molecular evolutionary genetics analysis version 7.0
375 for bigger datasets. *Molecular biology and evolution* **33**, 1870-1874 (2016).
- 376 28. A. Drozdetskiy, C. Cole, J. Procter, G. J. Barton, JPred4: a protein secondary structure prediction
377 server. *Nucleic acids research* **43**, W389-W394 (2015).
- 378 29. N. Eswar *et al.*, Comparative protein structure modeling using Modeller. *Current protocols in*
379 *bioinformatics* **15**, 5.6. 1-5.6. 30 (2006).
- 380 30. A. H. Maghrabi, L. J. McGuffin, ModFOLD6: an accurate web server for the global and local
381 quality estimation of 3D protein models. *Nucleic acids research* **45**, W416-W421 (2017).
- 382 31. W. L. DeLano, Pymol: An open-source molecular graphics tool. *CCP4 Newsletter On Protein*
383 *Crystallography* **40**, 82-92 (2002).
- 384 32. M. L. Dediego *et al.*, Pathogenicity of severe acute respiratory coronavirus deletion mutants in
385 hACE-2 transgenic mice. *Virology* **376**, 379-389 (2008).
- 386 33. B. Yount *et al.*, Severe acute respiratory syndrome coronavirus group-specific open reading
387 frames encode nonessential functions for replication in cell cultures and mice. *J Virol* **79**, 14909-
388 14922 (2005).
- 389 34. J. Soding, A. Biegert, A. N. Lupas, The HHpred interactive server for protein homology detection
390 and structure prediction. *Nucleic Acids Res* **33**, W244-248 (2005).
- 391 35. C. A. Nelson, A. Pekosz, C. A. Lee, M. S. Diamond, D. H. Fremont, Structure and intracellular
392 targeting of the SARS-coronavirus Orf7a accessory protein. *Structure* **13**, 75-85 (2005).
- 393 36. K. Hanel, T. Stangler, M. Stoldt, D. Willbold, Solution structure of the X4 protein coded by the
394 SARS related coronavirus reveals an immunoglobulin like fold and suggests a binding activity to
395 integrin I domains. *J Biomed Sci* **13**, 281-293 (2006).
- 396 37. J. M. Berg, J. L. Tymoczko, L. Stryer, L. Stryer, *Biochemistry*. (W.H. Freeman, New York, ed. 5th,
397 2002).
- 398 38. C. Ceraolo, F. M. Giorgi, Genomic variance of the 2019-nCoV coronavirus. *J Med Virol*, (2020).
- 399 39. S. El-Gebali *et al.*, The Pfam protein families database in 2019. *Nucleic Acids Res* **47**, D427-D432
400 (2019).
- 401 40. F. Ferron *et al.*, Structural and molecular basis of mismatch correction and ribavirin excision
402 from coronavirus RNA. *Proc Natl Acad Sci U S A* **115**, E162-E171 (2018).
- 403 41. A. Bateman, S. R. Eddy, C. Chothia, Members of the immunoglobulin superfamily in bacteria.
404 *Protein Sci* **5**, 1939-1941 (1996).
- 405 42. L. Aravind, E. V. Koonin, Gleaning non-trivial structural, functional and evolutionary information
406 about proteins by iterative database searches. *J Mol Biol* **287**, 1023-1040 (1999).
- 407 43. J. D. Mijnes *et al.*, Structure-function analysis of the gE-gI complex of feline herpesvirus:
408 mapping of gI domains required for gE-gI interaction, intracellular transport, and cell-to-cell
409 spread. *J Virol* **71**, 8397-8404 (1997).

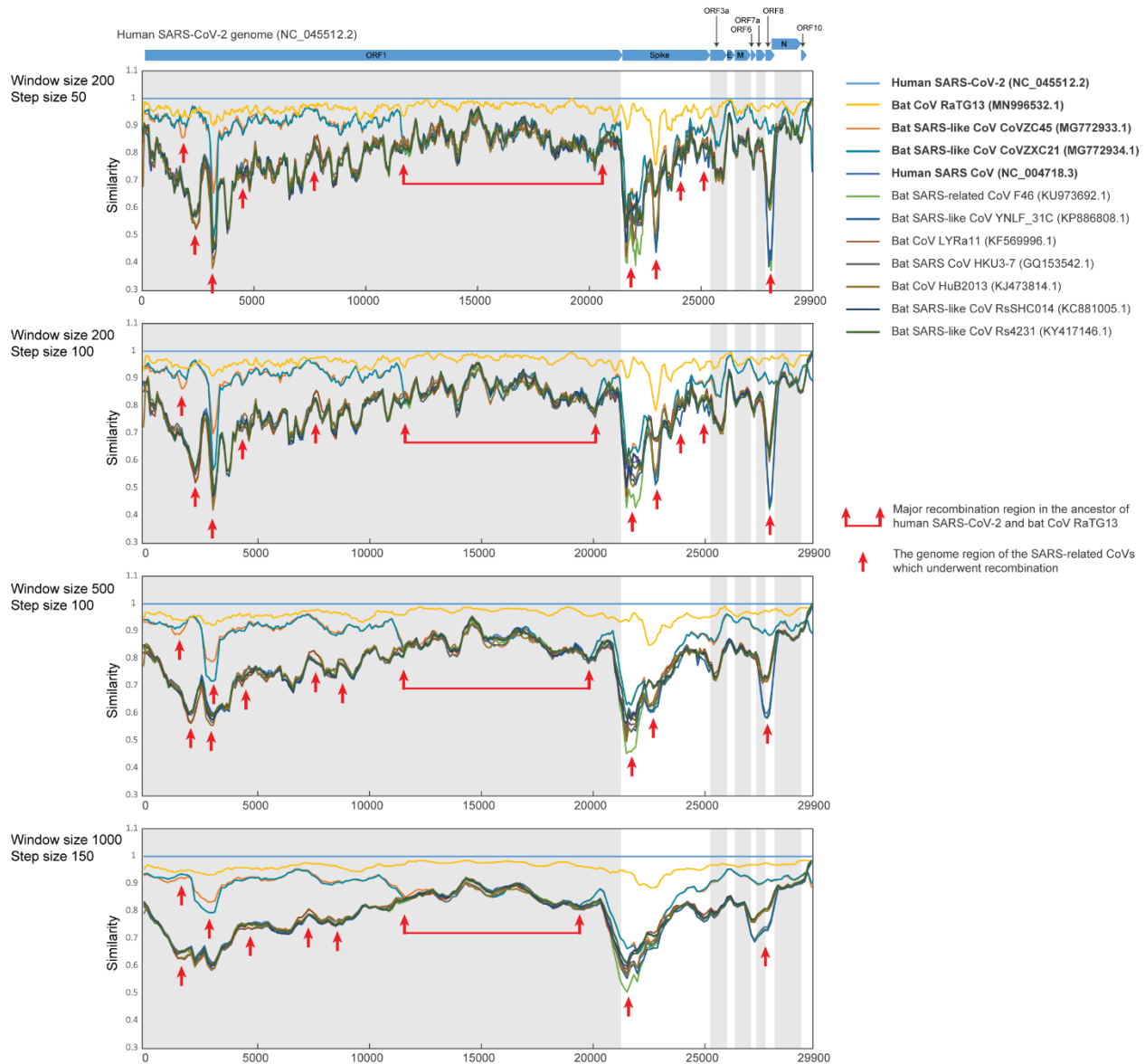
- 410 44. F. Deryckere, H. G. Burgert, Early region 3 of adenovirus type 19 (subgroup D) encodes an HLA-
411 binding protein distinct from that of subgroups B and C. *J Virol* **70**, 2832-2841 (1996).
- 412 45. H. S. Ginsberg *et al.*, Role of early region 3 (E3) in pathogenesis of adenovirus disease. *Proc Natl*
413 *Acad Sci U S A* **86**, 3823-3827 (1989).
- 414 46. R. H. Xu *et al.*, Antibody inhibition of a viral type 1 interferon decoy receptor cures a viral
415 disease by restoring interferon signaling in the liver. *PLoS Pathog* **8**, e1002475 (2012).
- 416 47. J. K. Taylor *et al.*, Severe Acute Respiratory Syndrome Coronavirus ORF7a Inhibits Bone Marrow
417 Stromal Antigen 2 Virion Tethering through a Novel Mechanism of Glycosylation Interference. *J*
418 *Viro* **89**, 11820-11833 (2015).
- 419 48. M. Oostra, C. A. de Haan, P. J. Rottier, The 29-nucleotide deletion present in human but not in
420 animal severe acute respiratory syndrome coronaviruses disrupts the functional expression of
421 open reading frame 8. *J Virol* **81**, 13876-13888 (2007).
- 422 49. S. K. Lau *et al.*, Severe Acute Respiratory Syndrome (SARS) Coronavirus ORF8 Protein Is Acquired
423 from SARS-Related Coronavirus from Greater Horseshoe Bats through Recombination. *J Virol* **89**,
424 10532-10547 (2015).
- 425 50. A. von Brunn *et al.*, Analysis of intraviral protein-protein interactions of the SARS coronavirus
426 ORF8. *PLoS One* **2**, e459 (2007).

427

428

SUPPLEMENTAL INFORMATION

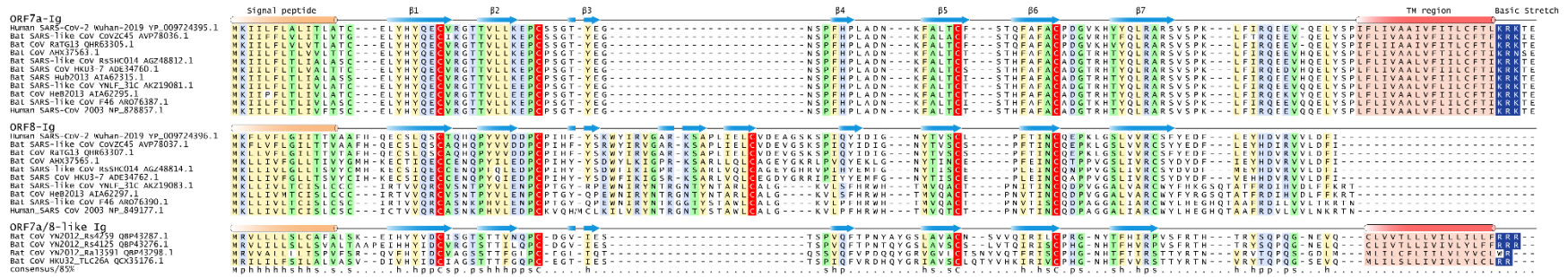
Supplementary Figure S1. Genome comparison analysis of SARS-related CoVs.



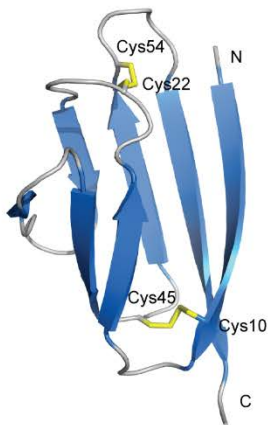
Similarity Plot of SARS-related CoVs against human SARS-CoV-2 Wuhan-Hu-1 genome (NC_045512.2) based on a multiple sequence alignment of the whole genomes. Each point represents a different slicing window size from the alignment with a different step size between each point. For each plot, the window size and step size are shown in the top left. Horizontal bars above the top plot correspond to the different open reading frames of the SARS-CoV-2 genome (NC_045512.2). Each different colored line corresponds to the nucleotide similarity between the human SARS-CoV-2 genome (NC_045512.2) and the respective SARS-related CoV genome. The red arrows and solid lines surround regions which display recombination within the SARS-related CoV genomes. The single red arrows point to specific regions of recombination.

Supplementary Figure S2. Full length multiple sequence alignment of ORF7a, ORF8-Ig and ORF7a/8-like proteins.

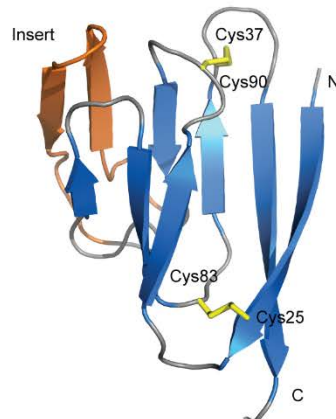
Each sequence in the MSA was labelled by its species abbreviation followed by its isolation and NCBI accession number. The predicted secondary structure is shown above the alignment and the consensus is shown below the alignment, where h stands for hydrophobic residues, s for small residues, and p for polar residues. The characteristic signal peptide, TM region and a stretch of basic residues are also labeled.



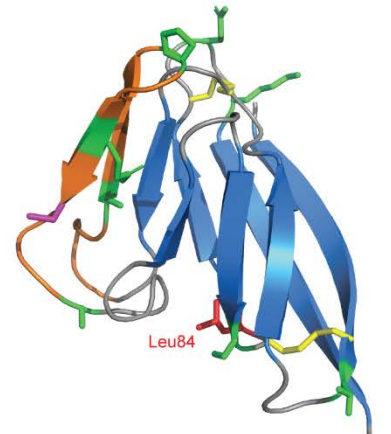
Supplementary Figure S3. Structural analysis of CoV Ig domains.



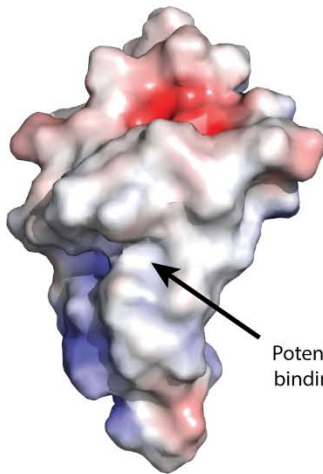
ORF7a-Ig domain
(PDB: 1xak_A)



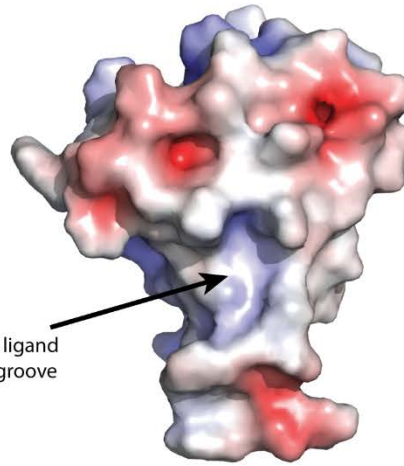
Model of ORF8-Ig domain



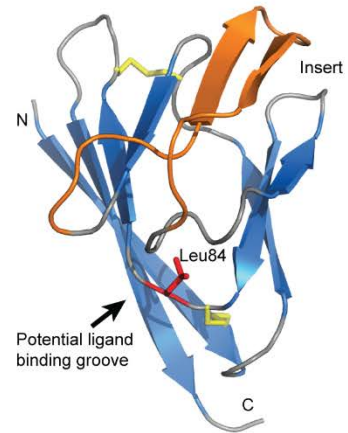
Location of highly variable
residues of ORF8-Ig domain
(sticks in green and red)



Surface view of ORF7a-Ig domain
(PDB: 1xak_A)



Surface view of ORF8-Ig domain



Location of hypervariable residue Leu84
on substrate-binding groove of the ORF8-Ig domain
(stick in red)

Supplementary Table S1. Detailed information of Human SARS-CoV-2 Wuhan-Hu-1 genome and other SARS-related genomes that were used in this study (Figure 1 & Figure S1).

Organism	Host	NCBI ID	Year	Citation
Severe acute respiratory syndrome coronavirus 2 (SARS-CoV-2) isolate Wuhan-Hu-1	Human	NC_045512.2	2020	A novel coronavirus associated with a respiratory disease in Wuhan of Hubei province, China (Unpublished)
Bat SARS-like coronavirus isolate bat-SL-CoVZC45	Bat	MG772933.1	2018	(1)
Bat SARS-like coronavirus isolate bat-SL-CoVZXC21	Bat	MG772934.1	2018	(1)
Bat coronavirus isolate RaTG13	Bat	MN996532.1	2020	Not Available
Severe acute respiratory syndrome-related coronavirus	Human	NC_004718.3	2003	(2)
Severe acute respiratory syndrome-related coronavirus isolate F46	Bat	KU973692.1	2017	Identification of a new intermediate virus between bat-CoVs and SARS-CoVs from least horseshoe bats in China (Unpublished)
Bat SARS-like coronavirus YNLF_31C	Bat	KP886808.1	2015	Not Available
Rhinolophus affinis coronavirus isolate LYRa11	Bat	KF569996.1	2014	(3)
Bat SARS coronavirus HKU3-7	Bat	GQ153542.1	2010	(4)
BtRs-BetaCoV/HuB2013	Bat	KJ473814.1	2015	(5)
Bat SARS-like coronavirus RsSHC014	Bat	KC881005.1	2013	(6)
Bat SARS-like coronavirus isolate Rs4231	Bat	KY417146.1	2017	(7)

Supplementary Table S2. Summary of representatives of viral Ig domain proteins which were identified in this study.

Family	Genus	Organism	NCBI ID	pfam ID	Domain Family	Presence of Signal Peptide (Y/N)*	Number of Ig-like domain	Number of TM region**	Distinct Relative PDB Structure#
Coronaviridae	Beta-coronavirus	SARS-CoV-2	YP_009724395.1	PF08779	SARS_X4	Y	1	1	1XAK_A
			YP_009724396.1	PF12093	Corona_NS8	Y	1	0	1XAK_A
		SARS-CoV	NP_828857.1	PF08779	SARS_X4	Y	1	1	1XAK_A
			NP_828876.1 NP_828877.1	PF08779	Corona_NS8	Y	1	0	1XAK_A
	Alpha-coronavirus	Bat coronavirus	QBP43259.1	n/a	Adeno_E3_CR1-like	Y	1	1	5XMZ_A
			QBP43265.1	PF08779	SARS_X4	Y	1	1	1XAK_A
Adenoviridae	Mast-adenovirus	Human adenovirus 7d	AAF14132.1	PF02440	Adeno_E3_CR1	Y	1	1	6JXR_d
		Human adenovirus 23	AFK92306.1	PF02440	Adeno_E3_CR1	Y	3	1	3J8F_7
		Human adenovirus 21	AAW33363.1	PF04881	Adeno_GP19K	Y	1	1	5IRO_P
Herpesviridae	Mardivirus	Gallid alphaherpesvirus 2	YP_001034013.1	PF02480	Herpes_gE	Y	1	1	2GJ7_F
			YP_001034012.1	PF01688	Herpes_gI	Y	1	1	5OR7_C
			YP_001033973.1	PF02124	Marek_A	Y	3	1	3J8F_7
	Simplexvirus	Macacine alpha-herpesvirus 1	NP_851925.1	PF01537	Herpes_glycop_D	Y	1	1	4MYV_A
	Rhadinovirus	Human gamma-herpesvirus 8	YP_001129350.1	PF02960	K1	Y	2	1	5D6D_C
	Cytomegalovirus	Panine beta-herpesvirus 2	NP_612760.1	PF16758	UL141	Y	1	1	4JMO_B
			NP_612778.1	PF05963	Cytomega_US3	Y	1	1	1IM3_P
			Human beta-herpesvirus 5	ABV71546.1	PF17622	UL16	Y	1	1
Aotine beta-herpesvirus 1			YP_004940175.1	PF08001	CMV_US	Y	1	2	1IM3_P
Poxviridae	Orthopoxvirus	Variola virus	NP_042191.1	PF08204	V-set_CD47	Y	1	5	5OR7_C
		Ectromelia virus	3OQ3_B	PF13895	ig	Y	3	0	3OQ3_B
Phenuiviridae	Goukovirus	Cumuto virus	YP_009664616.1	PF07245	Phlebovirus_G2	Y	4	1	6F8P_A 6EGU_B

* Signal Peptide Prediction was conducted by SignalP-5.0 program (8).

** Transmembrane (TM) region predictions were conducted by TMHMM Server (9).

The PDB structures which display similarity with the respective viral Ig domains identified by profile-profile comparisons (10).

REFERENCES

1. D. Hu *et al.*, Genomic characterization and infectivity of a novel SARS-like coronavirus in Chinese bats. *Emerging microbes & infections* **7**, 1-10 (2018).
2. M. A. Marra *et al.*, The genome sequence of the SARS-associated coronavirus. *Science* **300**, 1399-1404 (2003).
3. B. He *et al.*, Identification of diverse alphacoronaviruses and genomic characterization of a novel severe acute respiratory syndrome-like coronavirus from bats in China. *Journal of virology* **88**, 7070-7082 (2014).
4. S. K. Lau *et al.*, Ecoepidemiology and complete genome comparison of different strains of severe acute respiratory syndrome-related Rhinolophus bat coronavirus in China reveal bats as a reservoir for acute, self-limiting infection that allows recombination events. *Journal of virology* **84**, 2808-2819 (2010).
5. Z. Wu *et al.*, Deciphering the bat virome catalog to better understand the ecological diversity of bat viruses and the bat origin of emerging infectious diseases. *The ISME journal* **10**, 609-620 (2016).
6. X.-Y. Ge *et al.*, Isolation and characterization of a bat SARS-like coronavirus that uses the ACE2 receptor. *Nature* **503**, 535-538 (2013).
7. B. Hu *et al.*, Discovery of a rich gene pool of bat SARS-related coronaviruses provides new insights into the origin of SARS coronavirus. *PLoS pathogens* **13**, (2017).
8. J. J. A. Armenteros *et al.*, SignalP 5.0 improves signal peptide predictions using deep neural networks. *Nature biotechnology* **37**, 420-423 (2019).
9. A. Krogh, B. Larsson, G. Von Heijne, E. L. Sonnhammer, Predicting transmembrane protein topology with a hidden Markov model: application to complete genomes. *Journal of molecular biology* **305**, 567-580 (2001).
10. J. Söding, A. Biegert, A. N. Lupas, The HHpred interactive server for protein homology detection and structure prediction. *Nucleic acids research* **33**, W244-W248 (2005).